

Measuring Human-made Corner Structures with a Robotic Total Station using Support Points, Lines and Planes

Christoph Klug, Dieter Schmalstieg and Clemens Arth
Institute for Computer Graphics and Vision, Graz University of Technology,
Inffeldgasse 16/III, 8010 Graz, Austria

Keywords: Robotic Total Station, Reflectorless Electrical Distance Measurement.

Abstract: Measuring non-planar targets with a total station in reflectorless mode is a challenging and error-prone task. Any accurate 3D point measurement requires a fully reflected laser beam of the electronic distance meter and proper orientation of the pan-tilt unit. Prominent structures like corners and edges often cannot fulfill these requirements and cannot be measured reliably. We present three algorithms and user interfaces for simple and efficient construction-side measurement corrections of the systematic error, using additional measurements close to the non-measurable target. Post-processing of single-point measurements is not required with our methods, and our experiments prove that using a 3D point, a 3D line or a 3D plane support can lower the systematic error by almost a order of magnitude.

1 INTRODUCTION

Total stations are commonly used for measuring angles, distances and 3D points in surveying and building construction (Uren, 2010). A robotic total station, which can be remotely controlled, is equipped with an electronic distance meter (EDM), which uses a laser signal for accurate distance measurements¹. The simplified and calibrated geometric model of a common robotic total station without parallax effects between EDM and camera is shown in Fig. 1. In the ideal case, all coordinate systems are perfectly aligned: The EDM is aligned with the principal ray of the camera; the local spherical coordinate system of the instrument is aligned with the camera coordinate system, and the camera center is at the origin of the instrument coordinate system. Adjustment screws on the device allows an approximation of the ideal model, but for accurate measurements, an extended geometric model and device calibration is necessary. Such calibration includes camera parameters, temperature compensation and EDM corrections².

¹Details about EDM types can be found in (Amann et al., 2001).

²Details about extended geometric models, environmental influences and calibrations of total stations can be found in (Schulz, 2007; Uren, 2010; Nichols and Beavers, 2003; Coaker, 2009; Reda and Bedada, 2012; Martin and Gatta, 2006).

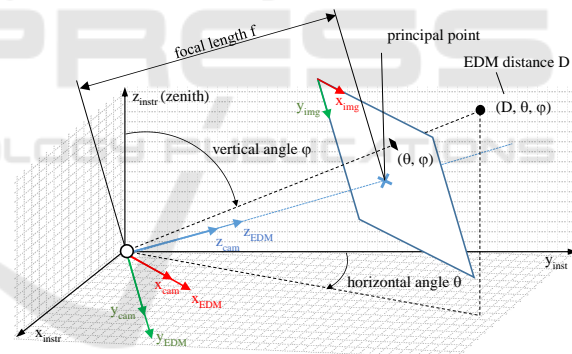


Figure 1: Simplified geometric model for a calibrated robotic total station with azimuth angle θ , polar angle ϕ and radial distance D . In this simplified version the coordinate system of the EDM is aligned with the camera coordinate system as well as the spherical coordinate frame robotic total station. Real-world devices require six degrees of freedom (DOFs) pose conversations between the coordinate frames as well as further corrections.

For standard measurements, reflective measurement targets with known calibration parameters are used. Modern total stations also support reflectorless measurements using the diffuse reflection of natural surfaces. This is often referred to as measuring natural targets. Common natural targets in surveying and building construction should have a high recall value, thus, preferred targets are corners and edges of human-made structures. Influences of the laser

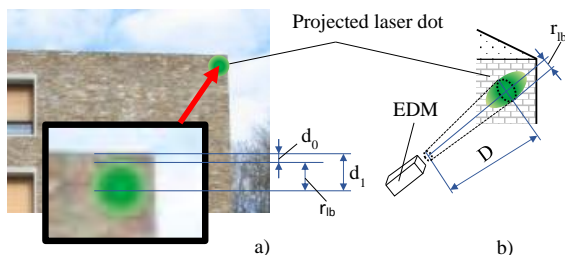


Figure 2: For a common reflectorless measurement target with one visible approximately planar surface, the laser dot must be fully reflected by the surface to get reliable distance results, precluding direct targeting of the corner. The minimum vertical and horizontal measurement error e is approximately defined by $e = d_0 + r_{lb}$, where d_0 is the *safety distance* between the edges of the target and the laser pointer, and r_{lb} is the radius of the projected laser beam (approximating the elliptical projection of the laser through a circle). d_0 is influenced by user experience, image resolution, focal length of the camera, image blur due to out-of-focus problems, back light conditions and other effects.

beam divergence of the EDM, angular resolution of the theodolite, inaccurate targeting and optical limitations are reasons why direct measurements of non-planar targets are critical and error-prone tasks. Surveyors often use post-processing methods to increase the accuracy of such measurements.

The wide variety of measurement conditions, the demanding requirements for the results of the measurement procedure regarding accuracy and reliability, and the aim to perform single-view metrology (Criminisi et al., 2000; Hartley and Zisserman, 2003) make multi-view photogrammetric algorithms largely inapplicable in realistic scenarios. Practical applications in indoor and outdoor environments can suffer from problems caused by sunlight and strong back-light, shadows, large distance measurements and partly occluded targets. All these issues are not fully solved problems in Computer Vision in general per se. Eventually the absence of multiple measurements and observations from multiple camera poses prohibits the usage of classic photogrammetry algorithms as such.

In this work, we therefore address the problem of reflectorless measuring targets with at least one quasi-planar surface visible to the total station (see Fig. 2), using three different methods. Post-processing and high density 3D point cloud scans are avoided to keep the measurement effort as low as possible. Since the projected laser dot should be fully located within the planar surface to avoid distance measurement errors, a systematic angular and distance error occurs, which depends on the projected laser dot size, the observation angle of the surface and other parameters³. With

³See Juretzko (Juretzko, 2004) for an extensive discus-

our algorithms, it is possible to reduce the systematic measurement error by applying image-based corrections directly in the field. As a side effect, the approach proposed simplifies the overall measurement procedure, such that even non-experts in the field can perform reliable and robust measurements. This is proven by the results of our pilot study.

2 RELATED WORK

In the following, we shortly review related work about using total stations for measuring.

The book by Uren (Uren, 2010) provides an extensive description of GPS measurements, total stations and laser range meters, explaining basic surveying and measurement methods, surveying hardware, software and tools, possible sources of errors and error propagations. Image-based measurement corrections are not described, however. Coaker (Coaker, 2009) investigated accuracy, precision and reliability of reflectorless total station measurement methods, also mentioning the problem of direct measurements of corners and edges. Similarly, Zeiske (Zeiske, 2004) describes basic surveying methods and offline corrections for 2D corner measurements using simple geometry. However, no online method or image-based geometric correction are mentioned.

Many modern total stations are already equipped with image-based measurement methods, like steering the total station to selected pixels, selecting and visualizing 3D targets in the image or visualizing metadata. Scherer *et al.* (Scherer, 2001; Scherer and Lerma, 2009) investigated possible benefits of image-based features for architectural surveying. The device of Topcon (Topcon Corporation, 2011) supports an image-based measurement feature for not directly measurable targets like corners and edges, but without providing any mathematical details or evaluation of the methods.

Ehrhart *et al.* (Ehrhart and Lienhart, 2015) investigate image processing methods for deformation monitoring. In their work they detect movements of complete regions by comparing image patches acquired with the camera of a total station, however, without explicitly performing any structural analysis of building corners or edges.

Siu *et al.* (Siu et al., 2013) describe a close range photogrammetric solution for 3D reconstruction and target tracking by combining several total stations and cameras. Jadidi *et al.* (Jadidi et al., 2015) use image based modelling to reconstruct 3D point clouds

of this problem.

and register as-built data to as-planned data. Fathi *et al.* (Fathi and Brilakis, 2013) generate 3D wire diagrams of a roof using video streams from a calibrated stereo camera set. Their algorithm combines feature point matching, line detection and a priori knowledge of roof structures to a structure from motion pipeline. Even if the results of these approaches are quite impressive, none of them can be applied for measuring corner and edge structures from a single position. Fathi *et al.* further notes accuracy problems of the reconstructed models.

Closely related to our approach is the work by Juretzko (Juretzko, 2004), who provides conceptual descriptions for not directly measurable target using intersections of 3D rays, lines and planes. However, no comparative study between the methods, no detailed mathematical description and no suitable user interface is provided. Furthermore, the author mentions only minimal measured point sets for each method without any model fitting approach.

To the best of our knowledge, we are the first to properly describe such measurement techniques with a detailed mathematical formalism, together with a comparative study. Moreover we are the first to investigate the measurement concept in detail in an outdoor scenario, giving results and insights into the issues arising outside of laboratory conditions in a practical working environment.

3 TEST HARDWARE AND LIMITATIONS

The total station we used for our experiments (see Fig. 3) had been fully calibrated by the manufacturer. It provides a closed source driver for controlling the device, for retrieving the camera image and for translating between all coordinate systems. As common for commercially available systems, there is no direct access to the raw data of the sensors, the geometric model and the related parameters. The applied correction algorithms are confidential and kept secret by manufacturers. While in our case the available API does not provide a projection matrix, it offers a complete API for coordinate system conversions. Therefore, we use the simplified geometric model, which is shown in Fig. 1, for a calibrated robotic total station to explain our methods.

Note that whether or not it is theoretically possible to perform full manual calibration for a single instance of a device at hand, it is neither reasonable to assume that every device is shipped with a calibration by the manufacturer that is perfect for each possible measurement situation, nor is manual calibration



Figure 3: Robotic Total Station and mobile PC used in our experiments. The communication between the devices is done wirelessly over WLAN.

easily possible given the level of access provided by APIs. Thus our assumption to work with the stock calibrated device *as is* and employing our simplified geometric model is plausible.

4 CONCEPT

We use the standard single point measurement method as reference method and define three new measurement methods, which integrate in-the-field corrections for corner and edge measurements:

- Direct reflectorless target measurement
- Reflectorless target measurement using a support point
- Reflectorless target measurement using a support line
- Reflectorless target measurement using a support plane

Figure 4 shows the direct measurement method as well as the support point, support line and support plane method. Details about the methods are provided in following sections.

4.1 Standard Method

When measuring a corner directly in reflectorless mode, the laser dot must be fully reflected by an attached surface. Fig. 1 shows the simplified geometric model for a single point measurement, while Fig. 2 shows the systematic error introduced by the aforementioned constraint.

Measurement Flow. The simple measurement flow is defined by following steps:

- Use the pan/tilt interface, until the target-of-interest is visible in the image
- Define target-of-interest in the image

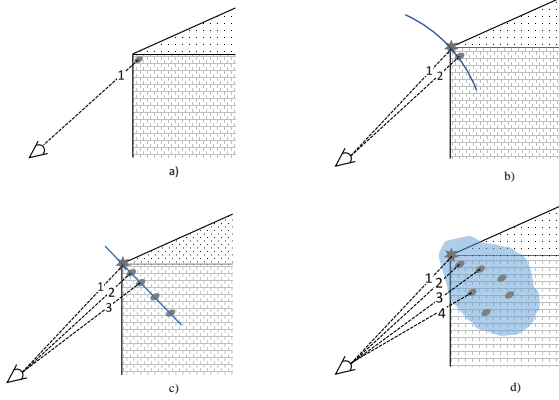


Figure 4: Four different measurement methods of a corner with a single visible adjacent area: direct method (a), support point method (b), support line method (c), support plane method (d). The numbers in the image indicate the minimum measurement count and the respective order used in our algorithms.

3. Calculate the 3D position of the target-of-interest by measuring the angle and distance at the selected image point

Calculating the Point. A total station defines a local spherical coordinate system. A point is defined by the horizontal angle φ , the vertical angle θ and the distance D . The simplified relation between spherical and Euclidean coordinates for our test device is given by following equations:

$$F(x, y, z) = \begin{pmatrix} D \\ \theta \\ \varphi \end{pmatrix} = \begin{pmatrix} \sqrt{x_i^2 + y_i^2 + z_i^2} \\ \arctan\left(\frac{x}{y}\right) = \text{atan2}(x, y) \\ \arccos\left(\frac{z}{\sqrt{x_i^2 + y_i^2 + z_i^2}}\right) \end{pmatrix} \quad (1)$$

with

$$D \geq 0 \quad -\pi \leq \theta < \pi \quad 0 \leq \varphi < \pi \quad (2)$$

Note that the azimuth angle φ is measured clockwise and is related to the Cartesian y direction rather than counterclockwise and related to the Cartesian x direction. This leads to swapped x and y variables in the expression $\text{atan2}(x, y)$ in Eqn. 1.

The inverse operation can be generalized to a 3D Euclidean rotation for a right-handed coordinate system:

$$Q(\theta, \varphi) = R_z(-\theta) \cdot R_y(0) \cdot R_x(-\varphi) \quad (3)$$

$$p = \begin{pmatrix} p_x \\ p_y \\ p_z \end{pmatrix} = G(D, \theta, \varphi) = Q(\theta, \varphi) \cdot \begin{pmatrix} 0 \\ 0 \\ D \end{pmatrix} \quad (4)$$

where p describes a 3D point in Euclidean coordinates and (D, θ, φ) describes a 3D point in spherical

coordinates; R_x, R_y, R_z are 3D rotation matrices in the Euclidean right-handed coordinate system around the x -axis, y -axis and z -axis, respectively. $Q(\theta, \varphi)$ is the combined rotation matrix which converts an angle measurement to an Euclidean space direction, here used for translating between local instrument coordinate system and camera coordinate system⁴. Eqn. 4 can easily be extended to non-aligned coordinate systems using homogeneous coordinates⁵.

We use spherical coordinates for storing selected 2D image positions to support rotation-invariant operations in the image space. Fig. 5 shows an image-based selection of a target in two different poses of the total station. To convert an image space coordinate to spherical coordinates, we first back-project the pixel coordinate into the camera space as view ray, convert to the instrument space and then apply Eqn.1 with $D = 1$. The instrument space is the local coordinate system. For our simplified model, the conversion is simply the inverse pose of the camera⁶.

The 3×4 camera projection matrix P can be split into the 3×3 matrix M and the 3×1 vector m

$$P = [M|m] \quad (5)$$

The back-projected ray \mathbf{X} can be written as

$$\mathbf{X}(\lambda, u) = P^\dagger \cdot u + \lambda \cdot C \quad (6)$$

where P^\dagger is the pseudo-inverse of the projection matrix P , u defines a 2D image coordinate and C is the camera center. For finite cameras, the following expression can be used, which avoids the calculation of the P^\dagger

$$\mathbf{X}(\mu, u) = \mu \begin{pmatrix} M^{-1} \cdot u \\ 0 \end{pmatrix} + \begin{pmatrix} -M^{-1} \cdot m \\ 1 \end{pmatrix} \quad (7)$$

This equation avoids a possible singularity of P^\dagger for camera center $C = 0$.

For our simplified model, the projection matrix as follows is calculated by

$$P = Q(-\theta, -\varphi) \cdot [K, C] \quad (8)$$

where θ, φ define the pose of the camera, K is defined by the intrinsic parameters of the camera and C is the camera center:

$$K = \begin{pmatrix} f_x & 0 & u_0 \\ 0 & f_y & v_0 \\ 0 & 0 & 1 \end{pmatrix} \quad C = \begin{pmatrix} 0 \\ 0 \\ 0 \end{pmatrix} \quad (9)$$

Note that the camera center C is aligned with the origin; f_x and f_y describes the focal length of the camera, u_0 and v_0 specify the principal point.

⁴A definition for the rotation matrices R_x, R_y, R_z can be

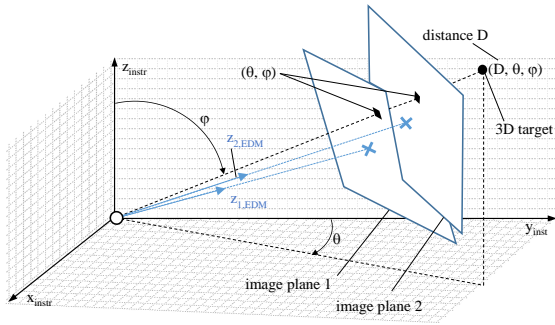


Figure 5: Using Spherical coordinates for image pixels enables rotation-invariant selection of 2D targets.

4.2 Support Point Method

To get the 3D coordinates of a building corner, the image pixel of the corner and a support point near the corner is defined, where the distance of the support point can be measured safely. Afterwards, the corner itself can simply be defined in the 2D image. The 3D coordinate of the target of interest is approximated by using the back-projected pixel of the first point and the measured distance of the support point. The approximation error becomes reasonable small for certain applications when following conditions hold: reasonable distance between the measurement device and the target, a perpendicular arrangement of the view ray and the measured surface, a small distance between the corner and the measured 3D point.

An offline version of this method is commonly used by surveying engineers (Coaker, 2009; Scherer, 2004; Juretzko, 2004). With the support point method, the minimal measurement count for a 3D point is $N_{min} = 1$. Fig. 4 shows the support point concept.

Measurement Flow. The simple measurement flow is defined by following steps:

1. Use the pan/tilt control interface, until the target-of-interest is visible in the image
2. Define target-of-interest in the image
3. Define support point with a single distance measurement
4. Calculate the 3D position of the target-of-interest by using the angle of the image point and the distance of the support point measurement

found in (Schneider and Eberly, 2003).

⁵In (Schneider, 2009; Schulz, 2007) a detailed description of the conversions is given.

⁶A robust method for calculating the ray given a 3×4 camera projection matrix is described in (Hartley and Zisserman, 2003).

Calculating the Point. In the user interface, two 2D image points are defined: the pixel coordinates of the target-of-interest u_1 and the pixel coordinates of the support point u_2 .

First both image points, u_1 and u_2 , are converted to spherical coordinates using Eqn. 6 with distance $\mu = 1$ and Eqn. 1 to get the control values for the EDM pose of the total station,

$$r_1 = \begin{pmatrix} r_{1,x} \\ r_{1,y} \\ r_{1,z} \end{pmatrix} = \mathbf{X}(1, u_1) \quad r_2 = \begin{pmatrix} r_{2,x} \\ r_{2,y} \\ r_{2,z} \end{pmatrix} = \mathbf{X}(1, u_2) \quad (10)$$

$$\begin{pmatrix} 1 \\ \theta_1 \\ \varphi_1 \end{pmatrix} = F(r_{1,x}, r_{1,y}, r_{1,z}) \quad \begin{pmatrix} 1 \\ \theta_2 \\ \varphi_2 \end{pmatrix} = F(r_{2,x}, r_{2,y}, r_{2,z}) \quad (11)$$

where r_1 and r_2 defines a back-projected point at distance $\mu = 1$.

Then the distance D_2 is measured with the EDM at the angle (θ_2, φ_2) using the API of the total station. Finally, we estimate the Euclidean 3D point x_1 of the back-projected image point u_1 using Eqn. 4 and the measured distance D_2 :

$$x_1 \approx G(D_2, \theta_1, \varphi_1) \quad (12)$$

4.3 Support Line Method

Several 3D points on the visible wall are measured by the user to estimate an 3D line which intersects the corner of interest. The corner itself can then simply be defined in the 2D image. The related 3D target is calculated by finding the intersection point of the back projected view ray with the previous estimated 3D doing with an least square approximation.

With support lines, the minimal measurement count for 3D points is $N_{min} = 2$. When using more than two points, a robust estimation like RANSAC based least square 3D line fitting can be applied (Fischler and Bolles, 1981). Fig. 4 shows the support line concept.

Measurement Flow. The simple measurement flow is defined by following steps:

1. Use the pan/tilt control interface, until the target-of-interest is visible in the image
2. Define target-of-interest in the image
3. Define support line with $N \geq 2$ measurements
4. Calculate the 3D position of the target-of-interest by intersecting the back-projected view ray with the support line

Calculating the Support Line. For $N = 2$ the 3D support line can be written directly as Eqn. 19. Fitting the 3D line for $N > 2$ can be separated into two steps: fitting the 3D line position and fitting the 3D line direction. First, the center of mass of the 3D points is subtracted:

$$x_i = (x_i, y_i, z_i)^T |_{i=0 \dots N-1} \quad \bar{x} = \frac{1}{N} \cdot \sum_{i=0}^{N-1} x_i \quad (13)$$

$$x'_i = x_i - \bar{x} |_{i=0 \dots N-1} \quad (14)$$

with \bar{x} as center of mass of the 3D point set. The translated 3D points x'_i are now centered around 0. Then, the 3D points are normalized:

$$k = \max(|x'_{x,i}|, |x'_{y,i}|, |x'_{z,i}|) |_{i=0 \dots N-1} \quad (15)$$

$$x''_i = \frac{x'_i}{k} |_{i=0 \dots N-1} \quad (16)$$

and the 3D line orientation is calculated by stacking points and solving the maximization problem:

$$A'' = \begin{pmatrix} x''_{x,0} & x''_{y,0} & x''_{z,0} \\ x''_{x,1} & x''_{y,1} & x''_{z,1} \\ \vdots & \vdots & \vdots \\ x''_{x,N-1} & x''_{y,N-1} & x''_{z,N-1} \end{pmatrix} \quad \max_{\|n\|=1} (|A'' \cdot n|) \quad (17)$$

The solution is the eigenvector which belongs to the largest eigenvalue and can be calculated by using SVD (Klasing et al., 2009). The line orientation is normalized for reasons of convenience:

$$n' = \frac{n}{\|n\|} = \begin{pmatrix} n'_x \\ n'_y \\ n'_z \end{pmatrix} \quad (18)$$

A 3D line is fully specified by an arbitrary point on the line and the orientation. For consistent calculations, the 3D orientation can be interpreted as 3D direction vector. Using the center of mass \bar{x} and the normalized line direction n' , the fitted 3D line \mathcal{L} in least square sense is given by

$$\mathcal{L}(t) = \bar{x} + t \cdot n' \quad (19)$$

Intersecting the View Ray with the Support Line.

First the 2D coordinate is back-projected to a 3D view ray using Eqn. 6. The best approximation for 3D line intersection can be found using Plücker coordinates (Hartley and Zisserman, 2003). However, we implemented 3D line intersection for two lines based on simple vector math (Schneider and Eberly, 2003).

4.4 Support Plane Method

To get the 3D coordinates of a building corner, the user measures several 3D points on the visible wall

to estimate an planar approximation of this wall. The corner of interest can simply be defined in the 2D image. The related 3D target is calculated by intersecting the back-projected view ray with the previous estimated plane. The measurement concept is shown in Fig. 4. The target-of-interest can be moved freely on the plane.

Measurement Flow. The simple measurement flow is defined by following steps:

1. Use the pan/tilt control interface, until the target-of-interest is visible in the image
2. Define target-of-interest in the image
3. Define support plane with $N \geq 3$ measurements
4. Calculate the 3D position of the target-of-interest by intersecting the back-projected view ray with the support plane

Calculating the Support Plane. In the easiest case the plane can be estimated by estimating the non-trivial solution of the linear homogeneous equation system

$$A \cdot p = 0 \quad A = \begin{pmatrix} x_{x,0} & x_{y,0} & x_{z,0} & 1 \\ x_{x,1} & x_{y,1} & x_{z,1} & 1 \\ \vdots & \vdots & \vdots & \vdots \\ x_{x,N-1} & x_{y,N-1} & x_{z,N-1} & 1 \end{pmatrix} \quad (20)$$

where A is a matrix of stacked homogeneous 3D points with a 3D point count $N = 4$. The plane parameters a , b , c and d of the implicit plane equation are given by the 4×1 vector

$$p = \begin{pmatrix} a \\ b \\ c \\ d \end{pmatrix} \quad p^T \cdot \begin{pmatrix} x_x \\ x_y \\ x_z \\ 1 \end{pmatrix} = 0 \quad (21)$$

where x_x , x_y , x_z are the coordinates of a 3D point on the plane.

Solving for p in Eqn. 20 for $N \geq 4$ becomes a constrained least squares minimization problem

$$\min_{\|p\|=1} (|A \cdot p|) \quad (22)$$

and can be solved with SVD (Klasing et al., 2009). A more robust plane estimation encounters some additional aspects:

- Minimal point set $N \geq 3$ instead of $N \geq 4$
- Normalization before computation for numerical stability
- RANSAC optimization for robustness against outliers in case of $N > 3$

For minimal point set, we must estimate the plane direction (rotation) and the plane translation separately. This procedure is analogous to the one for the support line, following Eqns. 13-18, but solving for the

eigenvector which belongs to the smallest eigenvalue. Finally, the implicit plane representation is given by

$$p = \begin{pmatrix} n'_x \\ n'_y \\ n'_z \\ -n'^T \cdot \bar{x} \end{pmatrix} \quad (23)$$

This method requires at least $N_{min} = 3$ measured 3D points.

Intersecting the View Ray with the Support Plane.

First, the 2D coordinate is back-projected to a 3D view ray using Eqn. 6. The target-of-interest is given by the plane-ray intersection

$$t = \frac{-(n'^T \cdot C + d)}{n'^T \cdot n_{ray}} \quad (24)$$

$$x_{target} = C + t \cdot n_{ray} \quad (25)$$

with n_{ray} as ray direction of the back projected image point, $C = 0$ as camera origin and $d = p(4)$ as distance between the origin and the intersection point (Schneider and Eberly, 2003). If the denominator of Eqn. 24 is zero, the ray is either parallel to the plane or lies directly on the plane.

5 EXPERIMENTS

We implemented the four methods described above and created a graphical user interface for a tablet computer, seamlessly interfacing the total station. The GUI shown in Fig. 6 is used to conveniently access the implementation and to enable even novice and non-expert users to use the methods in an intuitive way. Training time to introduce the concepts of measuring and the individual methods was thereby reduced to only around 10 minutes. After selection of the given method, the operator is automatically guided through the process to fulfill the measuring task, with a final result given at the end.

We defined a simple evaluation setup for prove-of-concept without the need of a laboratory for surveying and measurement. This setup can be applied in controlled indoor and in selected outdoor environments. Our analysis does not follow the ISO 17123 standard (ISO 17123-3:2001, 2001), since we conduct only a comparative studies of the proposed methods, where non-direct measurable targets are measured. We performed two different types of measurements, namely distance measurements and area measurements, and a number of laboratory and outdoor real-world experiments as follows.

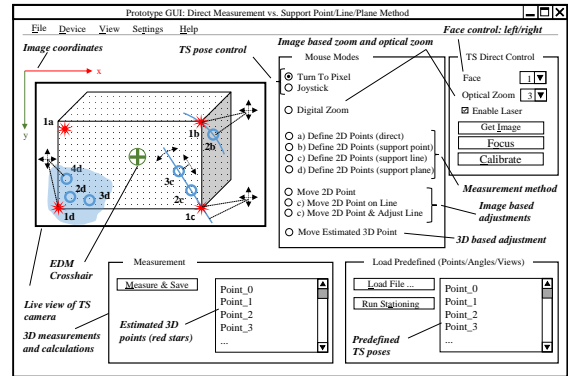


Figure 6: GUI used in our system. It enables intuitive selection of the method to use and guides the operator through the measurement process.

Measurement Setup. We measured the distance between two corners of a flat surface, whereby only the front face of the surface is fully visible. This is achieved by appropriately positioning the target and the total station:

- Approx. same height of target center and camera center
- Approx. perpendicular laser beam direction for laboratory experiments and outdoors for ground truth measurements
- Approx. perpendicular laser beam direction for ground truth measurements and 45° direction for outdoor evaluation

The measurement setup is shown in Fig. 7. The distance between the total station and the measurement target is about 5m in all experiments. The distance between the two top corners of the measurement indoor target is about 0.6m.

Measurement Strategy. For Euclidean distance evaluation, a single set measurement consists of the measured 3D position of the first and the second corner of the target⁷. All measurements were converted to Euclidean coordinates using the API of the device driver. The result is given in the confidence interval of $\pm 2\hat{\sigma}_d$, with $\hat{\sigma}_d$ as unbiased standard deviation assuming unbiased normal distribution of the measurements:

The Euclidean distance of measurement i between two points $p_{i,0}$ and $p_{i,1}$ is calculated by

$$d_i = \|p_{i,1} - p_{i,0}\| = \left\| \begin{pmatrix} x_{i,1} \\ y_{i,1} \\ z_{i,1} \end{pmatrix} - \begin{pmatrix} x_{i,0} \\ y_{i,0} \\ z_{i,0} \end{pmatrix} \right\| \quad (26)$$

and the average distance \bar{d} and the unbiased standard

⁷Note that we use a half-set for our evaluations, since we do not use the second telescope face (face right).

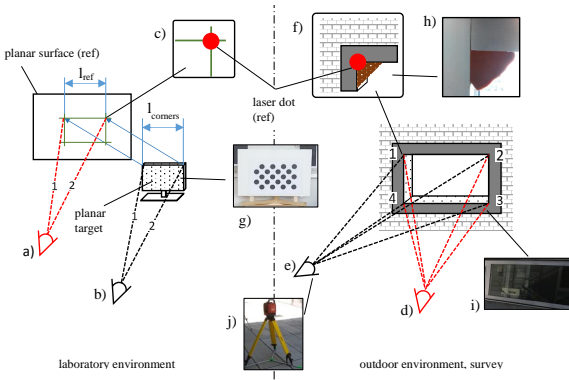


Figure 7: Measurement setups for laboratory conditions and for outdoor scenarios: a) measurement of the reference distance between the two top corners of the portable target, b) portable target used to measure the distance between two corners in laboratory conditions, c) detailed view of the projected laser dot during the reference measurement, d) reference measurement of a window in indoor and outdoor conditions using perpendicular viewing angle, e) the same windows measured with a viewing angle of 45 degree, f) and h) the modelling clay for reference measurements, i), j) and k) the outdoor window, the portable laboratory target and the robotic total station.

deviation $\hat{\sigma}$ is given by

$$\bar{d} = \frac{\sum_{i=0}^{N-1} d_i}{N} \quad \hat{\sigma} = \sqrt{\frac{\sum_{i=0}^{N-1} (d_i - \bar{d})^2}{N-1}} \quad (27)$$

For outlier removal, at least $N = 3$ sets must be measured. Outliers are removed using median absolute deviation (MAD) with $\pm 3\hat{\sigma}$ interval on distances (Leys et al., 2013). The statistic evaluation is repeated on the reduced data set.

We calculate the distance error between two points d using

$$\Delta d = |\bar{d}_{ref} - \bar{d}| \pm 2 \cdot \sqrt{\hat{\sigma}_{ref}^2 + \hat{\sigma}_1^2} \quad (28)$$

with $\bar{d}_{ref} \pm 2\hat{\sigma}_{dref}$ as reference distance and $\bar{d} \pm 2\hat{\sigma}$ as measured distances between two corners.

For area measurements, the area of a window in an outdoor environment was used as second method for indirect accuracy evaluation. A single set measurement for the area of the window consists of the the four measured 3D positions of the window corners. The area of an polygon in 3D can be calculated using the surveyor's area (Braden, 1986). For the four point case the calculation can be simplified to

$$A_i = \frac{1}{2} (|(p_{i,1} - p_{i,0}) \times (p_{i,2} - p_{i,0})| + |(p_{i,2} - p_{i,0}) \times (p_{i,3} - p_{i,0})|) \quad (29)$$

where A_i is the estimated area of the i^{th} measurement set and $p_{i,j}$ is the j^{th} estimated window corner of set i . We applied the same statistics on the areas A_i as provided for the distances d_i .

For measuring the ground truth, we employed two different approaches. For the laboratory target, we aligned it with a planar surface and measured the distance using the total station. Note that this method is suitable for portable targets and outer corners only. For ground truth estimation of immovable targets like windows, we filled the corners with modelling clay to create a quasi-planar surface around the corners, which could be measured by the total station. This method is suitable for fixed and portable targets and is well suited for inner corners⁸.

5.1 Laboratory Measurements

First, we conducted two experiments with the portable target. We measured the ground truth distance between the two top corners as shown in Fig. 7 a) and b). Then we used the four different methods to perform the measurement again, giving results as listed in the first group of rows in Tab. 1. The support line and support plane methods either outperform the others or perform on par.

In a second experiment, we measured the same distance again with the total station pointing at the target at an angle of approximately 45° . The results, given in the second group of rows in Tab. 1, indicate that the support line and support plane based methods achieve considerably better results than the standard method and the support point method.

Given a window as seen from the interior of a building, we performed four more experiments with a perpendicular and a viewing angle of 45° . First, we measured the distance between the two corners, then we measured the area of the window as shown in Fig. 7 d) and e). The results are given in group 3 and 4 of Tab. 1 and group 1 and 2 of Tab. 2 respectively. Overall, the support line and support plane based methods achieve considerably better results than the standard method and the support point method, or perform at least on par.

5.2 Outdoor Measurements

We conducted four outdoor experiments, where we measured the extents and the area of a window from a perpendicular and a 45° point of view. We measured

⁸Note that we performed the ground truth measurements immediately before the experiments, to ensure that errors due to changes in environmental conditions are negligible.

the ground truth distance and area as shown in Fig. 7 d), f) and h). Then, we applied the four measurement methods again. The results are shown in in group 5 and 6 of Tab. 1 and group 3 and 4 of Tab. 2. The support line and the support plane methods are overall more suitable and give better results, or perform at least on par.

5.3 Pilot Study

We asked a group of eight novice users and one expert user to perform all different methods on the task of measuring the distance of the upper two corners of an outdoor window and the area of the window, in analogy to the experiment described above. All users were introduced to the system, and all measurements with all methods were repeated three times.

Even for novice users with a short introduction to the system, the results for the support line and support plane method clearly outperform the standard method and the support point method, as indicated by the results listed at the bottom of Tab. 1 and Tab. 2 respectively.

The results in terms of the accuracy of the individual methods for the distance and the area measurements is depicted in Fig. 8. The line and the support plane method consistently and considerably outperform the standard and support point method, and, more importantly, all measurements have a considerably smaller variation.

The users were asked to complete a short questionnaire about the overall usability and the intuitiveness of the GUI and the overall approaches. The questions and the answers given by the users are summed in Tab 3. At a glance, users mainly voted for the support line and support plane method to be favorable over the standard and the support point method in terms of ease of use. Being asked about the usefulness of the three methods introduced in this work, users tended to favor the support line and the support plane method over the support line method. Concerning the accuracy and rapidness of the measurements, users preferred the plane support and the line support method, respectively.

6 DISCUSSION AND CONCLUSION

In this work, we have described different methods for indirect measurements using a total station. Based on the results of the experiments conducted, our methods consistently outperform the standard method, even when applied by novice users. One reason for the

Table 1: Distance measurements for experiments and methods: ground truth (r), direct targeting (a), support point (b), support line (c), support plane (d).

Record	Meth.	\bar{d} [m]	$\hat{\sigma}_d$ [m]	N	\bar{d}_{ref} [m]	$\Delta\bar{d}$ [m]
lab. 90°	(r)	600.191e-3	82.942e-6	4.000	600.191e-3	0
	(a)	586.664e-3	273.151e-6	4.000	600.191e-3	13.527e-3
	(b)	599.712e-3	39.655e-6	3.000	600.191e-3	478.897e-6
	(c)	599.803e-3	866.189e-6	5.000	600.191e-3	387.538e-6
	(d)	604.457e-3	3.636e-3	5.000	600.191e-3	4.266e-3
lab. 45°	(r)	600.191e-3	82.942e-6	4.000	600.191e-3	0
	(a)	582.446e-3	1.192e-3	5.000	600.191e-3	17.745e-3
	(b)	584.189e-3	240.581e-6	4.000	600.191e-3	16.002e-3
	(c)	598.194e-3	229.861e-6	3.000	600.191e-3	1.997e-3
	(d)	598.545e-3	654.487e-6	5.000	600.191e-3	1.646e-3
indoor 90°	(r)	881.992e-3	362.719e-6	10.000	881.992e-3	0
	(a)	893.240e-3	820.525e-6	8.000	881.992e-3	11.248e-3
	(b)	886.912e-3	1.921e-3	10.000	881.992e-3	4.920e-3
	(c)	887.088e-3	830.455e-6	10.000	881.992e-3	5.096e-3
	(d)	885.561e-3	957.555e-6	9.000	881.992e-3	3.569e-3
indoor 45°	(r)	881.702e-3	221.990e-6	5.000	881.702e-3	0
	(a)	897.636e-3	3.285e-3	5.000	881.702e-3	15.934e-3
	(b)	894.017e-3	2.142e-3	5.000	881.702e-3	12.314e-3
	(c)	882.071e-3	607.033e-6	5.000	881.702e-3	369.144e-6
	(d)	882.079e-3	1.165e-3	5.000	881.702e-3	377.119e-6
outdoor 90°	(r)	566.360e-3	20.239e-6	4.000	566.360e-3	0
	(a)	576.559e-3	351.065e-6	4.000	566.360e-3	10.199e-3
	(b)	565.040e-3	1.615e-3	5.000	566.360e-3	1.320e-3
	(c)	564.474e-3	32.128e-6	3.000	566.360e-3	1.886e-3
	(d)	564.664e-3	200.672e-6	4.000	566.360e-3	1.696e-3
outdoor 45°	(r)	2.192	107.789e-6	10.000	2.192	0
	(a)	2.196	1.182e-3	10.000	2.192	4.463e-3
	(b)	2.193	1.248e-3	10.000	2.192	1.761e-3
	(c)	2.189	819.832e-6	10.000	2.192	2.303e-3
	(d)	2.190	1.212e-3	10.000	2.192	1.587e-3
pilot study	(r)	2.192	107.789e-6	10.000	2.192	0
	(a)	2.214	14.497e-3	53.000	2.192	22.456e-3
	(b)	2.218	21.181e-3	53.000	2.192	26.853e-3
	(c)	2.188	4.148e-3	54.000	2.192	3.529e-3
	(d)	2.188	4.740e-3	54.000	2.192	3.406e-3

Table 2: Area measurements for different experiments and methods: ground truth (r), direct targeting (a), support point (b), support line (c), support plane (d).

Record	Meth.	\bar{d} [m]	$\hat{\sigma}_d$ [m]	N	\bar{d}_{ref} [m]	$\Delta\bar{d}$ [m]
indoor 90°	(r)	881.992e-3	362.719e-6	10.000	881.992e-3	0
	(a)	893.240e-3	820.525e-6	8.000	881.992e-3	11.248e-3
	(b)	886.912e-3	1.921e-3	10.000	881.992e-3	4.920e-3
	(c)	887.088e-3	830.455e-6	10.000	881.992e-3	5.096e-3
	(d)	885.561e-3	957.555e-6	9.000	881.992e-3	3.569e-3
indoor 45°	(r)	838.086e-3	37.490e-6	4.000	838.086e-3	0
	(a)	862.706e-3	1.079e-3	4.000	838.086e-3	24.620e-3
	(b)	854.846e-3	2.750e-3	5.000	838.086e-3	16.760e-3
	(c)	840.750e-3	20.712e-6	3.000	838.086e-3	2.663e-3
	(d)	839.188e-3	53.872e-6	3.000	838.086e-3	1.102e-3
outdoor 90°	(r)	883.245e-3	25.067e-6	4.000	883.245e-3	0
	(a)	888.800e-3	14.479e-6	3.000	883.245e-3	5.555e-3
	(b)	882.519e-3	807.959e-6	4.000	883.245e-3	726.362e-6
	(c)	881.964e-3	813.967e-6	5.000	883.245e-3	1.282e-3
	(d)	882.181e-3	249.838e-6	4.000	883.245e-3	1.065e-3
outdoor 45°	(r)	1.733	82.370e-6	5.000	1.733	0
	(a)	1.747	2.096e-3	5.000	1.733	13.809e-3
	(b)	1.737	2.827e-3	5.000	1.733	4.119e-3
	(c)	1.729	472.108e-6	4.000	1.733	4.515e-3
	(d)	1.731	632.497e-6	4.000	1.733	1.632e-3
pilot study	(r)	1.733	82.370e-6	5.000	1.733	0
	(a)	1.790	33.749e-3	27.000	1.733	56.605e-3
	(b)	1.751	13.249e-3	26.000	1.733	18.326e-3
	(c)	1.726	5.354e-3	27.000	1.733	6.882e-3
	(d)	1.727	5.486e-3	27.000	1.733	6.431e-3

huge gain in accuracy is due to the definition of the reference method, as the requirement that the projected laser beam has to be fully on the visible surface causes the big systematic error of the measurement method.

As a result of our experimental evaluation, we will further work on improving the individual methods to automatically detect outliers (*e.g.* by employ-

Table 3: Survey results for eight novice and one expert user concerning the ease, usefulness, accuracy and rapidness of the individual methods.

Question	Very easy [%]	OK [%]	Difficult [%]
How easy was it to use the DIRECT method?	55.6	22.2	22.2
How easy was it to use the POINT support method?	88.9	11.1	0
How easy was it to use the LINE support method?	100	0	0
How easy was it to use the PLANE support method?	100	0	0

Question	Yes [%]	Not sure [%]	No [%]
Do you think the POINT support method is useful?	44.4	44.4	11.1
Do you think the LINE support method is useful?	77.8	22.2	0
Do you think the PLANE support method is useful?	88.9	11.1	0

Question	Direct [%]	Point support [%]	Line support [%]	Plane support [%]
Which method do you prefer for ACCURATE measurements?	0	0	44.4	55.6
Which method do you prefer for FAST measurements?	11.1	22.2	44.4	22.2

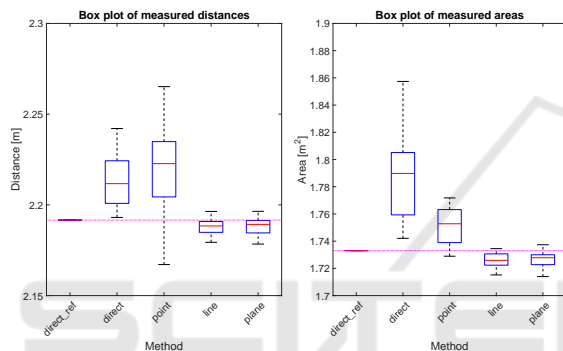


Figure 8: Pilot study results: distances between the two first window corners (left) and areas of the window (right) (outliers removed before evaluation). The plots show the median of the distance and area measurements, the lower and upper extremes, the 25th and the 75th percentile. The horizontal lines are the reference distance and area.

ing a RANSAC scheme on multiple measurements), and to further improve the GUI to more intuitively and automatically guide users through the measurement process.

We want to emphasize that, despite the basic algorithmic concepts are known for years, practical applications are still largely missing due to the issues arising in real measurement situations. As shown in this work, it is therefore highly relevant to study these concepts in practice to identify and overcome shortcomings of the underlying algorithms.

ACKNOWLEDGEMENTS

This work was funded by a grant from the Competence Centers for Excellent Technologies (COMET) 843272 with support from Hilti AG.

REFERENCES

- Amann, M.-C., Bosch, T. M., Lescure, M., Myllylae, R. A., and Rioux, M. (2001). Laser ranging: a critical review of usual techniques for distance measurement. *Optical Engineering*, 40(1):10–19.
- Braden, B. (1986). The Surveyor’s Area Formula. *The College Mathematics Journal*, 17(4):326.
- Coaker, L. H. (2009). Reflectorless Total Station Measurements and their Accuracy, Precision and Reliability. B.S. Thesis, University of Southern Queensland.
- Criminisi, A., Reid, I., and Zisserman, A. (2000). Single view metrology. *International Journal of Computer Vision*, 40(2):123–148.
- Ehrhart, M. and Lienhart, W. (2015). Image-Based Dynamic Deformation Monitoring of Civil Engineering Structures from Long Ranges. *Image Processing: Machine Vision Applications VIII*, 9405(1):94050J–94050J–14.
- Fathi, H. and Brilakis, I. (2013). A Videogrammetric As-Built Data Collection Method for Digital Fabrication of Sheet Metal Roof Panels. *Advanced Engineering Informatics*, 27(4):466–476.
- Fischler, M. A. and Bolles, R. C. (1981). Random Sample Consensus: A Paradigm for Model Fitting with Applications to Image Analysis and Automated Cartography. *Commun. ACM*, 24(6):381–395.
- Hartley, R. and Zisserman, A. (2003). *Multiple View Geometry in Computer Vision*. Cambridge University Press, Cambridge, UK New York.
- ISO 17123-3:2001 (2001). ISO 17123-3: Optics and optical instruments – Field procedures for testing geodetic and surveying instruments. Standard, International Organization for Standardization, Geneva, CH.
- Jadidi, H., Ravanshadnia, M., Hosseinalipour, M., and Rahmani, F. (2015). A Step-by-Step Construction Site Photography Procedure to Enhance the Efficiency of As-Built Data Visualization: A Case Study. *Visualization in Engineering*, 3(1):1–12.
- Juretzko, M. (2004). *Reflektorlose Video-Tachymetrie ein integrales Verfahren zur Erfassung geometrischer und visueller Informationen*. PhD thesis, Ruhr University Bochum, Faculty of Civil Engineering.
- Klasing, K., Althoff, D., Wollherr, D., and Buss, M. (2009). Comparison of surface normal estimation methods for range sensing applications. *2009 IEEE International Conference on Robotics and Automation*, pages 3206–3211.
- Lays, C., Ley, C., Klein, O., Bernard, P., and Licata, L. (2013). Detecting outliers: Do not use standard deviation around the mean, use absolute deviation around the median. *Journal of Experimental Social Psychology*, 49(4):764–766.
- Martin, D. and Gatta, G. (2006). Calibration of total stations instruments at the ESRF. *Proceedings of XXIII FIG Congress*, pages 1–14.
- Nichols, J. M. and Beavers, J. E. (2003). Development and Calibration of an Earthquake Fatality Function. *Earthquake Spectra*, 19(3):605–633.

- Reda, A. and Bedada, B. (2012). Accuracy analysis and Calibration of Total Station based on the Reflectorless Distance Measurement. Master's thesis, Royal Institute of Technology (KTH), Sweden.
- Scherer, M. (2001). Advantages of the Integration of Image Processing and Direct Coordinate Measurement for Architectural Surveying - Development of the System TOTAL. *FIG XXII International Congress*.
- Scherer, M. (2004). Intelligent Scanning with Robot-Tacheometer and Image Processing: A Low Cost Alternative to 3D Laser Scanning? *FIG Working Week*.
- Scherer, M. and Lerma, J. L. (2009). From the Conventional Total Station to the Prospective Image Assisted Photogrammetric Scanning Total Station: Comprehensive Review. *Journal of Surveying Engineering*, 135(4):173–178.
- Schneider, D. (2009). Calibration of a Riegl LMS-Z420i based on a multi-station adjustment and a geometric model with additional parameters. *The International Archives of the Photogrammetry, Remote Sensing and Spatial Information Sciences 38 (Part 3/W8)*, XXXVIII:177–182.
- Schneider, P. and Eberly, D. (2003). *Geometric Tools for Computer Graphics*. Boston Morgan Kaufmann Publishers, Amsterdam.
- Schulz, T. (2007). *Calibration of a Terrestrial Laser Scanner for Engineering Geodesy*. PhD thesis, ETH Zurich, Switzerland.
- Siu, M.-F., Lu, M., and AbouRizk, S. (2013). Combining Photogrammetry and Robotic Total Stations to Obtain Dimensional Measurements of Temporary Facilities in Construction Field. *Visualization in Engineering*, 1(1):4.
- Topcon Corporation (2011). *Imaging Station IS Series, Instruction Manual*.
- Uren, J. (2010). *Surveying for Engineers*. Palgrave Macmillan, Basingstoke England New York.
- Zeiske, K. (2004). Surveying made easy. https://www1.apis.anl.gov/files/download/DET/Detector-Pool/Beamline-Components/Lecia_Optical_Level/Surveying_en.pdf.